Original Research

Seed amplification assays for diagnosing synucleinopathies: the issue of influencing factors

Giovanni Bellomo[1,*], Silvia Paciotti[1], Leonardo Gatticchi[2], Domenico Rizzo[3,4], Federico Paolini Paoletti[1], Marco Fragai[3,4,5], Lucilla Parnetti[1,*]

[1]*Laboratory of Clinical Neurochemistry, Section of Neurology, Department of Medicine and Surgery, University of Perugia, 06132 Perugia, Italy,* [2]*Section of Physiology and Biochemistry, Department of Medicine and Surgery, University of Perugia, 06132 Perugia, Italy,* [3]*Magnetic Resonance Center (CERM), University of Florence, 50019 Sesto Fiorentino, Italy,* [4]*Department of Chemistry "Ugo Schiff", University of Florence, 50019 Sesto Fiorentino, Italy,* [5]*Consorzio Interuniversitario Risonanze Magnetiche MetalloProteine (CIRMMP), 50019 Sesto Fiorentino, Italy*

TABLE OF CONTENTS

1. Abstract
2. Introduction
3. Materials and methods
- *3.1 Kinetic modelling*
- *3.2 α-synuclein expression and purification*
- *3.3 Setup of seed amplification assays*
- *3.4 Preparation of preformed seeds*
- *3.5 Human CSF*
- *3.6 Data analysis software*

4. Results and discussion
- *4.1 Ab initio simulations*
- *4.2 Variables influencing α-synuclein seed amplification assays*

5. Conclusions
6. Author contributions
7. Ethics approval and consent to participate
8. Acknowledgment
9. Funding
10. Conflict of interest
11. References

1. Abstract

Background: The prion-like misfolding and aggregation of α-synuclein (α-syn) is involved in the pathophysiology of Parkinson's disease and other synucleinopathies. Seed amplification assays (SAAs) are biophysical tools that take advantage on the peculiar properties of prion proteins by amplifying small amounts of aggregates in biological fluids at the expense of recombinant monomeric protein added in solution. SAAs have emerged as the most promising tools for the diagnosis of synucleinopathies *in vivo*. However, the diagnostic outcome of SAAs depends on the aggregation kinetics of α-syn, which in turn is influenced by several experimental variables. **Methods**: In our work, we analysed the impact on SAAs of some of the most critical experimental factors by considering models that describe the aggregation kinetics of α-syn. **Results**: We started our analysis by making simulations to understand which kinetic models could explain the aggregation kinetics of α-syn during incubation/shaking cycles. Subsequently, under shaking/incubation cycles similar to the ones commonly used in SAAs, we tested the influence of some analytical variables such as monomer concentration, presence/absence of glass beads, pH, addition of human cerebrospinal fluid, and use of detergents on α-syn aggregation. **Conclusions**: Our investigation highlighted how optimization and standardization of experimental procedures for α-syn SAAs is of utmost relevance for the ultimate goal of applying these assays in clinical routine. Although these aspects have been evaluated with specific SAA protocols, most of the experimental variables considered influenced very general aggregation mechanisms of α-syn, thus making most of the results obtained from our analyses extendable to other protocols.

Submitted: 6 August 2021 Revised: 6 October 2021 Accepted: 26 October 2021 Published: 30 November 2021

2. Introduction

Parkinson's disease (PD), the most common neurodegenerative movement disorder, is pathologically characterized by the presence, in selectively vulnerable brain regions, of intracytoplasmic and axonal inclusions, called Lewy bodies and Lewy neurites, which consist of aggregates of misfolded α-synuclein (α-syn), crowded organelles and lipid membranes [1, 2]. Accumulation of insoluble fibrillary α-syn is usually accompanied, both as a cause and a consequence, by the impairment of the autophagy-lysosomal pathway, which represents one of the main mechanisms involved in the intracellular degradation of α-syn [3]. Diagnosis of PD can be challenging in the early disease stages when only non-motor prodromal symptoms (i.e., hyposmia, REM sleep behavioural disorders, constipation and mood disturbances) are present, sometimes associated with slight and ambiguous motor signs, which often lead to misdiagnosis. The long prodromal phase of PD [4] provides the possibility for early therapeutic intervention, once disease-modifying therapies will be developed. However, the lack of biomarkers for early diagnosis and for monitoring disease progression represents a major obstacle to the achievement of this goal. Cerebrospinal fluid (CSF) levels of total α-syn [5], oligomeric α-syn [6], phosphorylated α-syn [6], protein deglycase DJ-1 [7], amyloid-β 1-42 [7], tau [8], and lysosomal enzymes activities [9, 10] are candidate biomarkers for PD although they still show low specificity and sensitivity for PD and other synucleinopathies [5, 11–13]. With respect to this, oligomeric and fibrillary aggregates of α-syn are found to spread from cell to cell as well as in CSF [14–16]. This evidence makes the detection of misfolded α-syn in CSF a promising strategy for the early diagnosis of PD. At the same time, the understanding of the "prion-like" behaviour of α-syn provided new perspectives for the development of novel diagnostic assays. Indeed, two seed amplification assays (SAAs) [17], namely protein misfolding cyclic amplification (PMCA) [18] and real-time quaking-induced conversion (RT-QuIC) [19], have been successfully applied for the detection of misfolded prion protein (PrPSc) in tissues and biological fluids of animals [20–22] and humans [23]. PMCA and RT-QuIC currently represent the best option to perform the diagnosis of prion diseases, such as Creutzfeldt-Jacob disease, in CSF [23] and other peripheral fluids and tissues [24, 25]. These assays have been recently adapted for the detection of prone-to-aggregation α-syn in CSF [26–33].

In α-syn SAAs, biological samples collected from patients are incubated with recombinant α-syn and subjected to phases of incubation and shaking which are cyclically alternated at fixed temperatures. During incubation, oligomeric/protofibrillary α-syn, possibly present in the biological samples collected from patients affected by synucleinopathies, grow by recruiting the recombinant monomeric α-syn substrate. During vigorous shaking, large aggregates are disrupted into smaller subunits, which in turn are able to grow at the expense of the monomers present in solution [33]. This process finally results in an exponential amplification of the α-syn aggregates originally present in the biological matrix under exam. In α-syn SAAs, the aggregation process is generally monitored in real-time with a fluorescent dye (generally thioflavin-T, ThT) which intercalates to the β-sheet motifs of aggregated species. In different investigations, α-syn SAAs showed high sensitivity and specificity in differentiating PD from healthy controls and from non-α-syn-related parkinsonisms by using CSF as biological matrix [26–33]. Some other accessible peripheral matrices, such as olfactory mucosa [34, 35] and skin biopsies [36–38], also produced very encouraging results. Considering the impact that SAAs might have when introduced in PD diagnostic workup, the analysis of the effects of experimental variables on the α-syn aggregation kinetics is a crucial step for both optimization and standardization of these experimental protocols. In our work, we analysed the impact of critical experimental factors such as concentration of monomeric α-syn substrate, presence and quantity of glass beads, pH, addition of human CSF and addition of detergents.

3. Materials and methods

3.1 Kinetic modelling

Kinetic modelling was performed to highlight the most contributing mechanisms of α-syn aggregation in SAAs. The differential equations used are displayed in the Results & Discussion sections. Equations were integrated as previously described with minor modifications [39]: the Euler solver was replaced with a more performant Runge-Kutta solver, the code used for the simulations was run on Python 2.7 instead of C++, a varying fragmentation kinetics was applied to accurately simulate the intermittent shaking of SAAs, oligomeric populations were not considered since SAAs amplification processes mostly involve fibrils and protofibrils.

3.2 α-synuclein expression and purification

Escherichia Coli BL21(DE3) Gold were transformed with pT7-7 vector cloned with the gene encoding α-syn. The overnight preculture of transformed cells was diluted 100-fold in Luria-Bertani medium and induced at an OD_{600} value of 0.6–0.8 with 1 mM Isopropyl-β-D-thiogalactoside and, after 5 h incubation at 37 °C, the cells were harvested at 4000 rpm (JA-10, Beckman Coulter, Fullerton, CA, USA). The extraction was carried out through osmotic shock using 100 mL of buffer TRIS 30 mM, EDTA 2 mM and sucrose 40%, at pH 7.2 according to Shevchik *et al.* [40] and Huang *et al.* [41]. The suspension was then ultracentrifuged at 20000 rpm (Type 70 Ti rotor, Beckman Coulter, Fullerton, CA, USA) for 25 min

and pellet was collected and resuspended with 90 mL pre-cooled ultrapure water additioned with 38 μL of $MgCl_2$ 1 M and then ultracentrifuged a second time. Supernatants derived from these two centrifugation steps, were joined and dialyzed against 4 litres of buffer 20 mM TRIS/HCl at pH 8.0. The protein then was loaded in the FPLC system and an anion exchange chromatography was carried out with 0–50% linear gradient of NaCl 1 M (GE Healthcare HiPrep™ Q HP 16/10 Column). The collected fractions were lyophilized and resuspended in 10 mM TRIS/HCl, 1 mM EDTA and urea 8 M at pH 8.0 for the chemical denaturation. To eliminate all the protein formed aggregates, two size-exclusion chromatographies (HiLoadTM 16/600 SuperdexTM 75 pg Column) were performed with 20 mM phosphate and 0.5 mM EDTA at pH 8.0 as elution buffer. Purified α-synuclein (α-syn) was dialyzed against Milli-Q water and lyophilized in batches for long-term storage. The purity of the monomeric α-syn was evaluated by SDS-PAGE. Roche cOmplete™ protease inhibitor cocktail was added only during the extraction step in the quantity suggested by the producer.

3.3 Setup of seed amplification assays

Lyophilized aliquots of α-syn were resuspended in NaOH 3.5 mM (pH 11.5) right before the experiments to avoid the instantaneous formation of aggregates. At high pH, the negatively charged monomers (the isoelectric point of α-syn is 4.67) experience an electrostatic repulsion that impedes the aggregation and favours the dissociation of small aggregates [42, 43]. The α-syn solution was then brought to the desired pH by adding concentrated buffers (PIPES or phosphate buffers, depending on the experiment). In all the reaction buffers used, ThT was present at a concentration of 10 μM together with NaN_3 (0.08%). Each sample/condition analysed was replicated in three distinct wells in clear-bottom 96-well plates (TECAN©, #30122306). We added acid-washed glass beads in each well, of different size and number depending on the experiment, to enhance the aggregation speed and increase homogeneity among replicates. The plates were always sealed with a sealing tape to minimize evaporation during the experiments. Plates were inserted in a BMG LABTECH *ClarioStar* fluorimeter and subjected to the incubation/shaking protocol of Shahnawaz *et al*. [27] (T = 37 °C, 29 min incubation, 1 min double-orbital shaking at 500 rpm). While testing the effect of detergent we used conditions more similar to the ones of protocols making use of it [28, 29, 44] by using α-syn 0.08 mg/mL in phosphate buffer (40 mM) pH 7.4 + 170 mM NaCl, 6 $\times$ 1 mm diameter glass beads and 15 μL of CSF for a final volume of 100 μL per well. Cycles of 1 min shaking (500 rpm double orbital) and 1 min rest at 42 °C were used. Once every 30 minutes, the fluorescence was read from the bottom using an excitation and emission wavelength of 450 nm and 480 nm, respectively.

3.4 Preparation of preformed seeds

Monomeric α-syn at the concentration of 2 mg/mL was incubated in 100 mM PIPES buffer with 500 mM NaCl at 37 °C in two wells (250 μL per well) of a 96-wells plate, under constant agitation at 500 rpm. One of the two wells contained 10 μM ThT in order to monitor the aggregation. Once the plateau of the ThT aggregation profiles was reached (usually after seven days), the sample without ThT was subjected to cycles of sonication, using an immersion sonicator, in order to obtain smaller aggregates (5 cycles of 15 seconds sonication at 12 μm oscillation amplitude and 15 seconds rest). The solution containing the preformed aggregates was then split in aliquots, diluted to the desired concentrations, and stored at –80 °C for later use. One aliquot was analysed by Western blot (details of the procedure used in **Supplementary Fig. 1**, Supplementary Material) to evaluate the pattern of the obtained aggregates (**Supplementary Fig. 1**, Supplementary Material).

3.5 Human CSF

To avoid problems related to biological variance of CSF samples, CSF aliquots from a single female hydrocephalic patient of 67 years old were used in this work. This patient showed no cognitive or motor impairment. Lumbar puncture was performed according to international guidelines [45, 46]. Following a standardized procedure, 12 mL of CSF were collected in a sterile polypropylene tube and centrifuged at room temperature for 10 min (2000$\times$ g). Aliquots (0.5 mL) were frozen at –80 °C. In the CSF sample used, the core Alzheimer's disease biomarkers were measured using Lumipulse G600-II (Lumipulse) β-Amyloid 1–40, Lumipulse β-Amyloid 1–42, Lumipulse Total Tau and Lumipulse p-Tau 181 assays (Fujirebio Europe, Gent, Belgium), resulting in a profile not compatible with the presence of Alzheimer's disease with all measured biomarkers falling within the normal range.

3.6 Data analysis software

To extract the position of inflection points, ThT fluorescence profiles were fitted with Boltzmann's sigmoidal functions by using the non-linear fitting routine of OriginPro 9.0. Linear regression analyses were performed with the linear regression tool of Microsoft Excel.

4. Results and discussion

4.1 Ab initio simulations

We started our analysis by making simulations to understand the simplest kinetic model that could explain the aggregation kinetics of α-syn during incubation/shaking cycles. We wanted to reproduce the linear relations initially observed by Shahnawaz *et al*. [27] and by Arosio *et al*., [47] between the $t_{1/2}$ (time to the half of the maximum value) and the logarithm of the seed (preformed aggregates) mass

$$\frac{df_i(t)}{dt} = k_n m(t)^{n_0}\delta_{i,n_0} - k_{on}m(t)f_i(t) + k_{on}m(t)f_{i-1}(t) - k_{off}f_i(t) + k_{off}f_{i+1}(t) - k_{frag}(t)(i-1)f_i(t) + 2k_{frag}(t)\sum_{j=i+1}^{\infty} f_j(t)$$

$$P_f(t) = \sum_{i=n_0}^{\infty} f_i(t) \quad ; \quad M_f(t) = \sum_{i=n_0}^{\infty} i f_i(t)$$

$$\begin{cases} \frac{dP_f(t)}{dt} = k_{frag}(t)\left[M_f(t) - (2n_0 - 1)P_f(t)\right] + k_n m(t)^{n_0} \\ \frac{dM_f(t)}{dt} = \left(m(t)k_{on} - k_{off} - k_{frag}(t)n_0(n_0 - 1)\right)P_f(t) + +n_0 k_n m(t)^{n_c} \\ m(t) = m_0 - M_f(t) \end{cases}$$

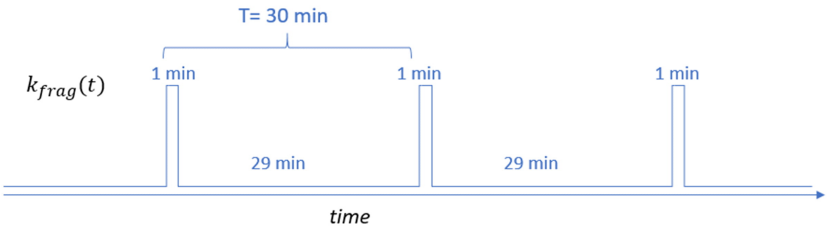

Fig. 1. Description of the kinetic model used to interpret the aggregation of α-syn under intermittent shaking. In the model of differential equations used for the simulations, the fragmentation rate varies according to the incubation/shaking cycles of the SAA protocol. f(i) = population of fibrils made by i monomers; k_n= primary nucleation rate; m(t) = monomer population; n_0 = size of the smallest nucleus (i.e., 2); δ_{ij} = Kronecker's delta function; k_{on} = fibril polymerization rate; k_{off} = fibril depolymerization rate; k_{frag}(t) = variable fragmentation rate; P_f(t) = fibril total population; M_f(t) = fibril total mass concentration; m_0 = initial monomer mass concentration.

concentration. A nucleated polymerization model (Fig. 1) [48, 49] with intermittent fragmentation (Fig. 1) could produce an approximate linear relation (Fig. 2). In this model, secondary nucleation was not included [50]. Indeed, the rates of the secondary nucleation processes during α-syn aggregation have a strong pH dependence. Indeed, it has been previously shown that starting from pH 6, secondary nucleation provides a minor contribution in the aggregation kinetics of α-syn [51].

The simulated range of seed masses shown in Fig. 2 is arbitrary and not related to experimental values. The range of seed masses, for which it is possible to obtain this linear relation depends on the kinetic constants of the processes, which themselves depend on the nature of the protein-protein interaction and on experimental variables like temperature, pH, shaking cycles, protein concentrations and ionic strength. Optimizing the experimental variables, to maximize the differentiation between seed masses, is the first step in developing SAAs for the diagnosis of synucleinopathies.

4.2 Variables influencing α-synuclein seed amplification assays

We evaluated the impact on α-syn aggregation of different experimental factors such as the addition of glass beads, starting monomer concentration, solution pH, size and number of glass beads, addition of human CSF and use of detergents.

The addition of glass beads to wells containing Thioflavin-T (ThT) and monomeric α-syn is reported in literature to be beneficial for reducing the fibrillization time and for increasing the homogeneity among replicates [52, 53]. In the simplified model that we described in Fig. 1, at t = 0 the formation of novel fibrillar species is dependent on the nucleation and fragmentation kinetics. By increasing the latter, through sonication/vigorous shaking in the presence of beads, seeding should be favoured with respect to unspecific nucleation of aggregates. To verify this hypothesis, we performed tests on equivalent samples with and without glass beads. In Fig. 3, we reported the ThT fluorescence profiles of α-syn samples with 20 ng of seeds, subjected to a SAA protocol, without (Fig. 3A) and with (Fig. 3B) glass beads. To quantify the variability among replicates we used the maximum coefficient of variation (MCV), calculated as the maximum value of the ratio between standard deviation and mean fluorescence value of the three replicates during the course of the experiment. The replicates in Fig. 3A produced smooth fluorescence lineshapes, with high variability among replicates (MCV = 0.68). At 160 h, none of the replicates reached the final fluorescence plateau. Conversely, the replicates in Fig. 3B produced noisier fluorescence lineshapes but with less variability among replicates (MCV = 0.36). All the replicates reached the final fluorescence plateau in about 100 h. Similar results were obtained by repeating the experiment with and without glass beads with 2 ng of seeds (**Supplementary Fig. 2**, Supplementary Material, MCVs of 0.36 and 0.69, respectively).

A second experiment was performed to evaluate the impact of different size and number of glass beads in three different buffers, the results are shown in Fig. 4. From this image, it is possible to appreciate that a single bead of 3 mm of diameter produced a faster aggregation with respect to 17 beads with a diameter of 0.5 mm. Moreover, for any

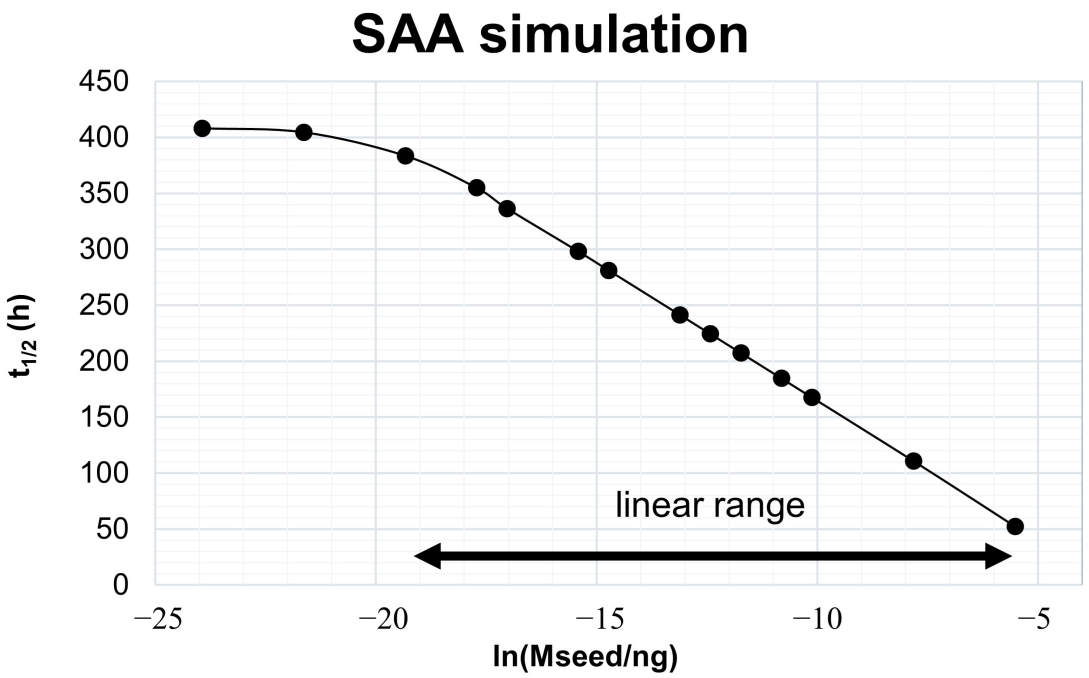

Fig. 2. Kinetic model-derived relation between aggregate mass and $t_{1/2}$. By numerically integrating the differential equation system shown in Fig. 1 with a Runge-Kutta solver, it was possible to extract the $t_{1/2}$. In this way, it was possible to demonstrate the existence of a range of preformed aggregates (seeds) concentrations (starting from arbitrary kinetic constants) in which the relation between the logarithm of the initial mass of the seeds per ng and the $t_{1/2}$ of the "sigmoidal" growth of the fibrillary species was approximately linear.

beads size and number, the aggregation of α-syn was faster in PBS pH 7.4 compared to PBS pH 8.2 and even faster in 100 mM PIPES pH 6.5 + NaCl 500 mM. These results are in accord with the fact that, starting from pH 4.5 (the isoelectric point of α-syn), the C-terminus of α-syn becomes negatively charged at increasing pH [42, 54], which results in an electrostatic repulsion between monomers and between monomers and preformed aggregates. Conversely, pH values near the isoelectric point of α-syn neutralize charge repulsion and promote conformational changes, which results in an increased aggregation proneness [55, 56].

CSF coming from a single hydrocephalus subject not suffering from neurodegenerative diseases was subsequently added to the reaction mix. In this way, we could test the different analytical variables on different aliquots from the same subject without introducing effects linked to biological variance. The detection limit and the ability to differentiate among seed masses were tested by adding in-lab made preformed aggregates (seeds) in different quantity in each well, the protocol used to produce α-syn seeds is reported in the Materials and Methods section. The incubation/agitation protocol (29 min incubation, 1 min shaking at 500 rpm) and the reaction buffer (100 mM PIPES buffer pH 6.5 with NaCl 500 mM) of Shahnawaz and coworkers [27] were used for all the experiments described in Figs. 5,6,7 and 8. For this protocol we also analysed wells containing seeds and CSF without recombinant α-syn to determine whether the addition of seeds could produce a significant increase in fluorescence by itself. The results of this experiment are shown in **Supplementary Fig. 4** (Supplementary Material). In summary, we did not observe any significant change produced by the addition of seeds in the absence of monomeric α-syn.

In Fig. 5A are reported the kinetic traces, averaged on three replicates for each seed quantity, relative to a SAA performed with 17 glass beads (diameter of 0.5 mm) per well. Interestingly, the addition of human CSF produced a delay in the aggregation of α-syn (Fig. 5A). This phenomenon was previously observed [27, 57, 58] and, although not being fully understood, it could be produced by the interaction between α-syn and CSF protein constituents [42, 59]. From Fig. 5A and from Fig. 3, it can be appreciated the fact that most of the fluorescence profiles have two inflection points: a first inflection point, situated between 0 h and 25 h and a second one, situated between 60 h and 70 h. The presence of two inflection points in most of the observed ThT profiles indicates a two-step process occurring during the SAA. The presence of the second inflection point may be explained by the transition from the initially amplified oligomeric/proto-fibrillar aggregates into well-structured fibrils. This type of transition produced similar trends in aggregation assays involving α-syn [60, 61] and amyloid-β [39]. According to this hypothesis, the seeded samples in Fig. 5 (which exhibit a higher fluorescence intensity at the first plateau), may have had a higher percentage of prefibrillar aggregates with respect to unseeded ones. Indeed, apart from fibrillary aggregates the added seeds contained also oligomeric/proto-fibrillar

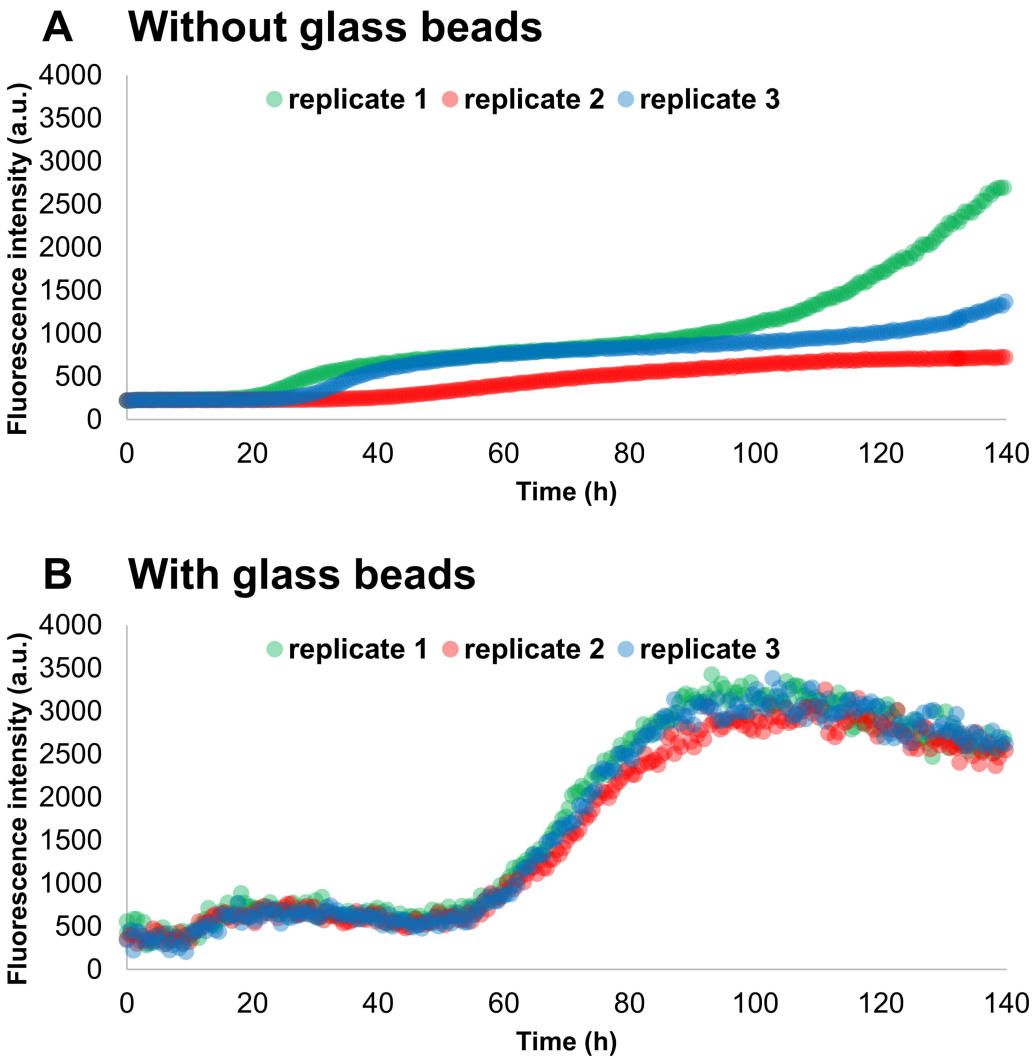

Fig. 3. The addition of glass beads increases the reproducibility among replicate samples in SAAs. Monomeric α-syn 0.125 mg/mL (8.7 μM) was left aggregating in the presence of ThT 10 μM and 0.2 ng of preformed seeds. The experiments were performed in triplicate in a 96-wells plate in 100 mM PIPES buffer pH 6.5 (with 500 mM NaCl). The SAA protocol consisted in cycles of 1 min shaking at 500 rpm (double orbital) and 29 min rest at 37 °C, in (A); no glass beads were added while, in (B), 17 × 0.5 mm diameter glass beads were added to the samples.

species (**Supplementary Fig. 1**, Supplementary Material) which may have been initially amplified in the first hours of the experiment. The drop in fluorescence after reaching the maximum value (e.g., in Fig. 5A) often occurs in protein aggregation assays and is thought to be produced by the formation of insoluble macroscopic aggregates, capable of trapping ThT molecules [62].

To accurately measure the position of the first inflection point (t_0), the first parts of the aggregation profiles were fitted with a Boltzmann's sigmoidal function (Eqn. 1), using. In the non-linear curve fitting procedure used, the parameters A_1, A_2, t_0 and dt of Eqn. 1 were let free. With reference to Fig. 2, t_0 coincides with $t_{1/2}$when A_2 = 0, i.e., when the initial fluorescence intensity is negligible.

$$y(t) = A_2 + \frac{A_1 - A_2}{1 + \exp\left(\frac{t - t_0}{dt}\right)} \quad (1)$$

The results of the fitting are shown in Fig. 5B. The measured t_0 parameters were then plotted against the natural logarithm of the mass (per ng) of the added seed. From the linear regression shown in Fig. 5C, it can be appreciated that there is a good linearity between the t_0 parameters (R2 ~ 1) and the natural logarithm of the seed mass, as was expected from simulations and previous investigations [27, 47]. The linear response was maintained up to 0.02 pg (0.1 pg/mL) of seeds, which coincides with the detection limit of this protocol.

The assay optimization promoted the "seeded" aggregation and limited the spontaneous aggregation of the

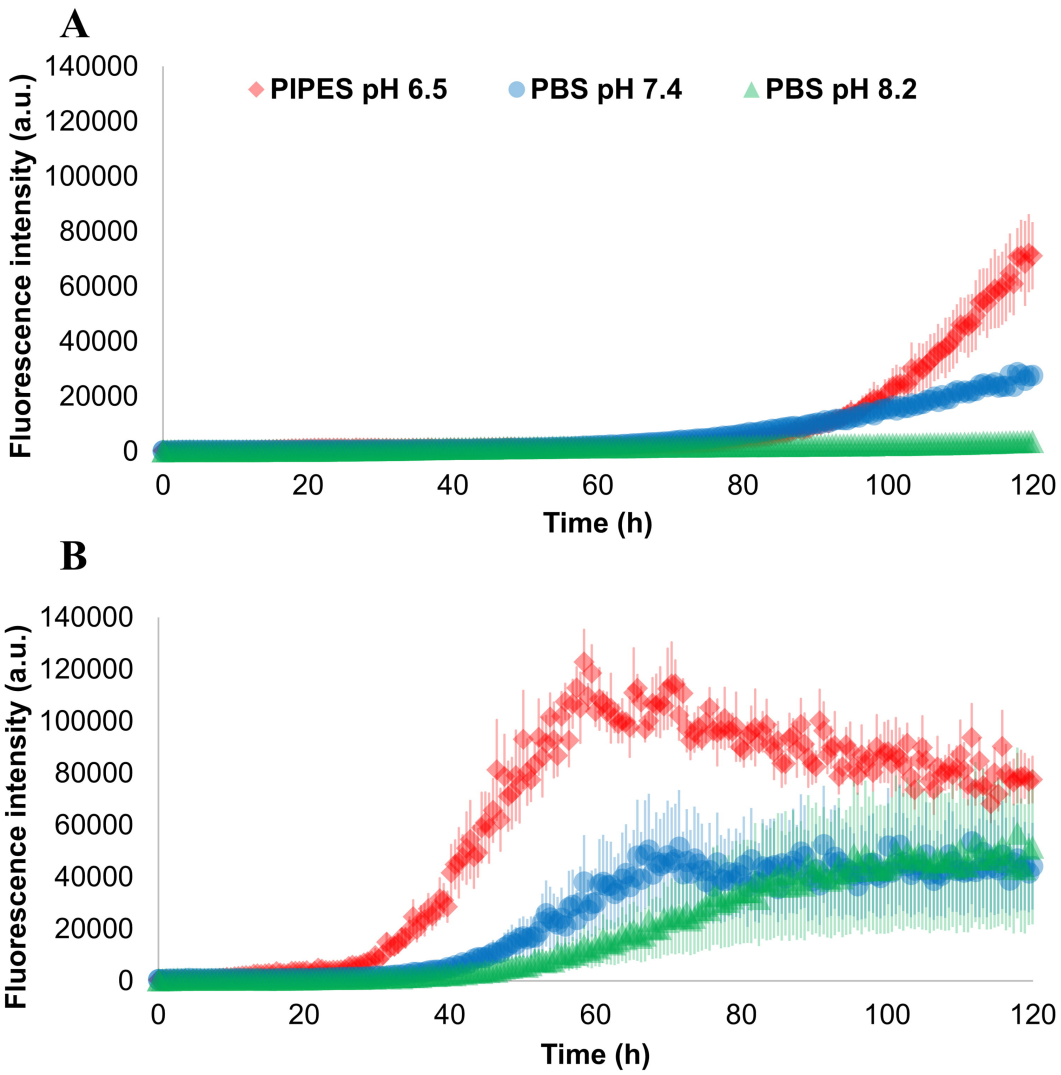

Fig. 4. Effect of different buffers and beads on α-syn aggregation in SAAs. Monomeric α-syn 0.08 mg/mL (6.9 μM) was left aggregating in the presence of ThT 10 μM and 20 ng of preformed seeds. The experiments were performed in a 96-wells plate in three different buffers: 100 mM PIPES buffer pH 6.5 (with 500 mM NaCl), PBS buffer pH 7.4 and PBS buffer pH 8.2. The SAA protocol consisted in cycles of 1 min shaking at 500 rpm (double-orbital) and 29 min rest at 37 °C. In (A), 17 glass beads with a diameter of 0.5 mm were added: in (B), a single bead with a diameter of 3 mm was added to the samples. The data shown are the averages of three replicates while the error bars represent the standard error of the mean fluorescence value on replicates. Single kinetic traces relative to this experiment are shown in **Supplementary Fig. 3** (Supplementary Material).

free monomer to obtain the maximum possible differentiation of the masses of the added seeds. From the linear regression of Fig. 5C, it is possible to notice that, although the R2 coefficient is almost equal to 1, the slope of the line was low, which represented the fact that the first inflection point of the aggregation profiles laid in a short range of time (5 h–20 h) for all the curves. In a second trial, we lowered the monomer concentration from 0.125 mg/mL to 0.08 mg/mL. This choice was made to discourage the primary nucleation kinetics, which, according to the model described in Fig. 1, depends on the square of the monomer concentration while the polymerization kinetics of the fibrils depends linearly on that. Also, the number of beads was slightly reduced from 17 to 15 to ameliorate the signal to noise ratio of each curve to allow a better fitting of the first plateau. As before, we analysed the first part of the aggregation curves extracting the t_0 parameters with the sigmoidal fitting (Fig. 6A) but we tried also to estimate the so-called *lag-time* to quantify the time at which the fluorescence starts to deviate significantly from its initial value. We defined it, in a similar way to the one used by Groveman *et al.* [28], as the time at which the fluorescence ()F of each well becomes higher than the average fluorescence of the first 10 h ($\overline{F\,(t)}_{t<10\ h}$) of the sample without seeds plus 5 standard deviations (5σ) for 5 consecutive measurements:

$$F\,(t_{lag}+i\Delta t) \geq \overline{F(t)}_{t<10h} + 5\sigma(F(t))_{t<10h}; \forall i \in (0,1,2,3,4) \quad (2)$$

Where iΔts the time between two consecutive measure-

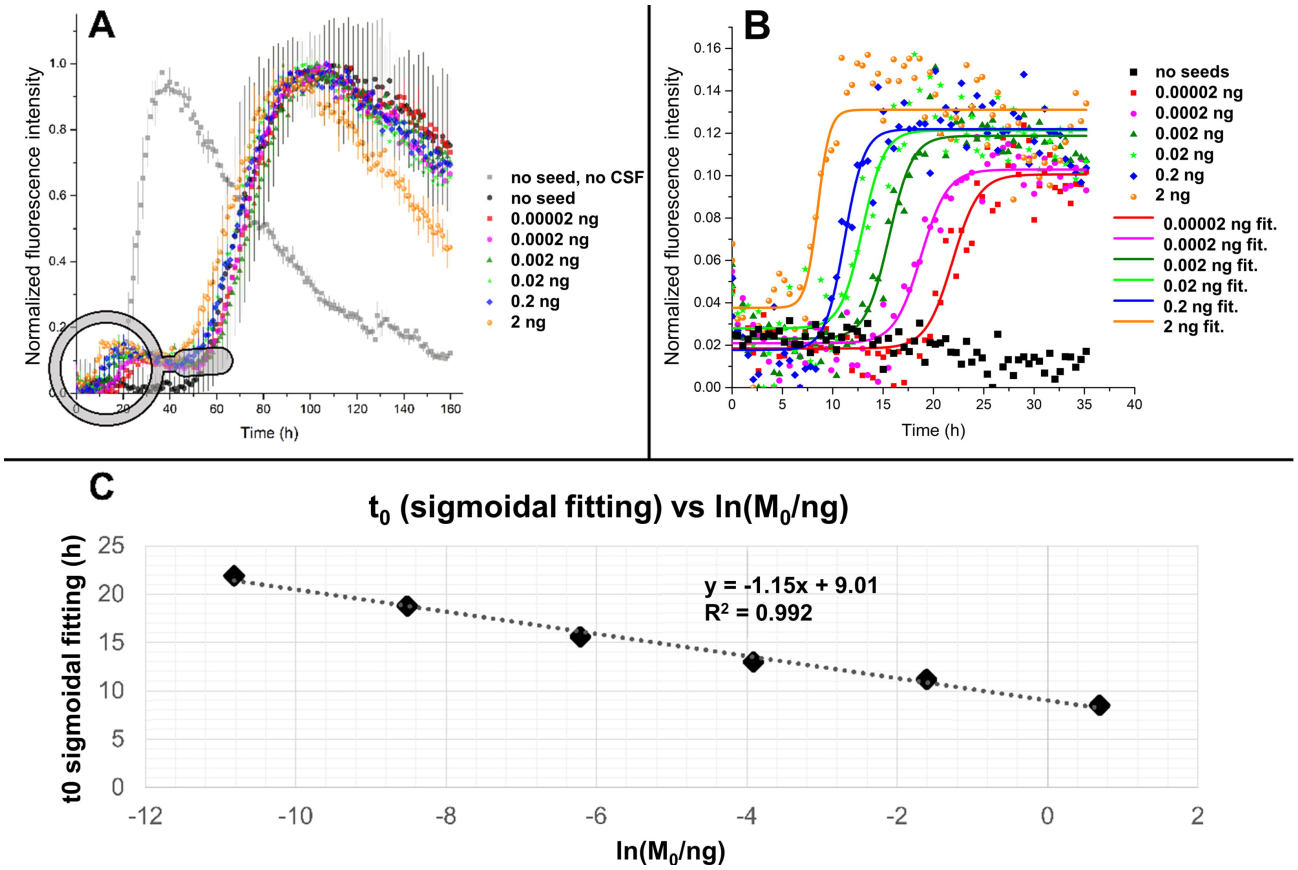

Fig. 5. Fitting of ThT profiles in the presence of human CSF and preformed seeds. (A) SAA performed using 0.125 mg/mL of recombinant α-syn in 100 mM PIPES pH 6.5 (500 mM NaCl) with 40 μL of CSF (final volume of 250 μL) in the presence of different quantities of preformed aggregates and 17 glass beads with a diameter of 0.5 mm. The data shown are the averages of three replicates on a 96-wells plate while the error bars represent the standard error of the mean fluorescence value on replicates. (B) The first part of the aggregation curves was fitted with a Boltzmann's sigmoidal function to extract the position t_0 of the inflection point. (C) The measured t_0 values were plotted against the natural logarithm of the added quantity of seed and fitted with a linear function.

ments (30 min in our case). The inverse of the lag-time, the lag-rate, is usually used in the SAA protocols to visualize the data, since it provides a faster and easier way to examine together the outcome of multiple experiments with respect of plotting the fluorescence profiles for all the samples in the same graph (an example of this representation is provided in Fig. 6C. Moreover, as it is defined in Eqn. 2, the estimation of lag-times does not necessarily need to reach a fluorescence plateau, making lag-times measurable also for incomplete kinetic traces. The averages of the lag-times (estimated with the threshold method of Eqn. 2) on three replicates were plotted against the natural logarithm of the seed masses per ng, the result of the linear regression procedure is shown in Fig. 6D.

The R2 values and the slopes of the linear regressions for the t_0 values and the lag-times were similar, as expected, with the slope being more than twice the one calculated in Fig. 5C. The tested protocol was still able to differentiate seed masses with a detection limit of 0.02 pg. In Fig. 7, it is reported a summary of the measured t_0 values for different bead sizes and two initial monomer concentrations. The t_0 parameters were calculated both on the first and on the second inflection points in the same conditions in Fig. 7A and in Fig. 7B.

All the tested conditions produced satisfactory differentiations between seed masses with a good linear correlation between the measured t_0 parameters and the logarithm of the added seed masses. By looking at Fig. 7B and Fig. 7C, it is possible to notice that, as expected from the considerations on the nucleation and polymerization kinetics, the samples with a starting monomer concentration of 0.08 mg/mL produced an increased slope compared to the ones with 0.16 mg/mL, even though the overall experiment duration was also longer. The second inflection point showed also to be discriminative for the 0.16 mg/mL monomer concentration, as can be seen from Fig. 7A, while for the 0.08 mg/mL monomer concentration it was still not reached after 250 h. The increased number of beads, with respect to Fig. 5 and Fig. 6, produced slightly noisier lineshapes but neither a significative increase in the aggregation speed nor in seed mass discrimination. However, by substituting the 21 beads with a diameter of 0.5 mm with a sin-

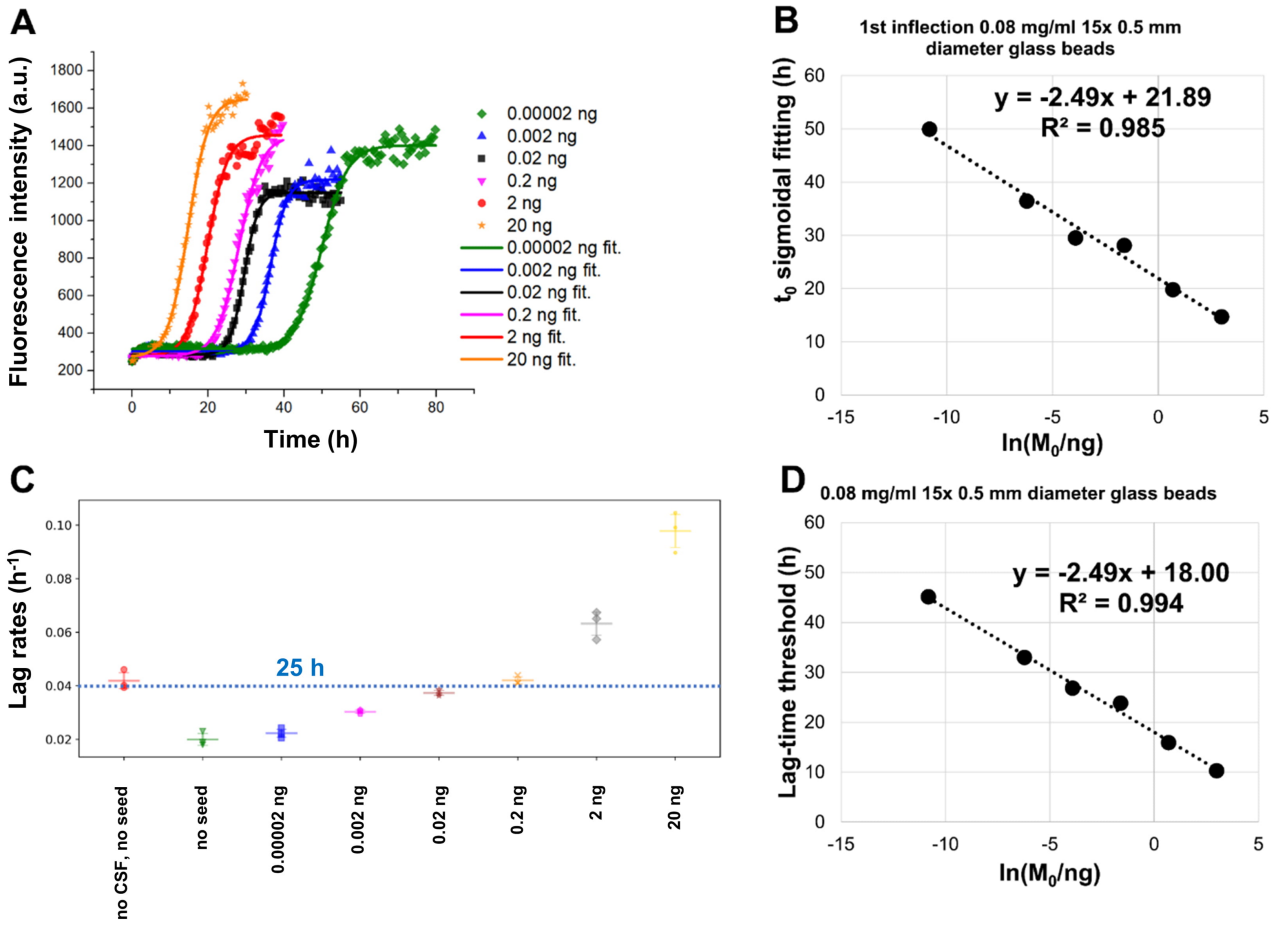

Fig. 6. Performance of fitted t_0 and lag-time in differentiating among preformed seed masses. SAA performed using 0.08 mg/mL of recombinant α-syn in 100 mM PIPES pH 6.5 (500 mM NaCl) with 40 μL of CSF (final volume of 250 μL), in the presence of different quantities of preformed aggregates and 15 glass beads with a diameter of 0.5 mm. (A) The first part of the aggregation curves, averaged on the three replicates, was fitted with a Boltzmann's sigmoidal function to extract the position t_0 of the inflection point. (B) The measured t_0 values were plotted against the logarithm of the added quantity of seed and fitted with a line. (C) The lag-rates are calculated as the inverse of the lag-times for each sample. (D) The measured lag-times, averaged on the three replicates, were plotted against the logarithm of the added quantity of seed and fitted with a linear function.

gle bead with a diameter of 3 mm (the total bead mass is ~ 10 times greater) we observed the almost disappearance of the first inflection point (Fig. 8A), probably due to the more rapid transition from oligomeric/protofibrillary species into fibrils. The t_0 values and the lag-times measured for this kinetics produced good results in terms of R2 and slope of the linear regression, as can be seen from Fig. 7D and from Fig. 8B.

Another variable that emerged in some protocols present in literature [28, 44, 58, 63] is the presence of detergents, such as *Sodium Dodecyl Sulphate* (SDS), which is commonly used in the RT-QuIC/PMCA protocols for the detection of PrPSc.

For these experiments, 2 μL of a stock solution (PBS containing 3 different SDS concentrations) were added to the reaction mix. The lag times were evaluated for each well using the formula in Eqn. 2 by considering the average fluorescence of the first 5 h instead of 10 h due to the high aggregation propensity of samples containing seeds and a final SDS concentration of 0.01%. We tested the addition of SDS in conditions more similar to the ones of protocols making use of it [28, 29, 44] by using α-syn 0.08 mg/mL in phosphate buffer (40 mM) pH 7.4 + 170 mM NaCl, 6 $\times$ 1 mm diameter glass beads and 15 μL of CSF for a final volume of 100 μL per well. Cycles of 1 min shaking (500 rpm double orbital) and 1 min rest at 42 °C were used. A slightly lower pH and higher shaking rpm with respect to the one of published protocols were needed to promote aggregation probably due to the different shaking efficiency of our fluorimeter compared to *BMG Omega*. As can be evinced from Table 1, the addition of SDS dramatically accelerated the aggregation kinetics of α-syn both in seeded and unseeded experiments. The SDS-induced fibrillization of α-syn was previously documented by Otzen and coworkers [58] and it is currently used to increase the speed and reproducibility of screening assays to measure the effects

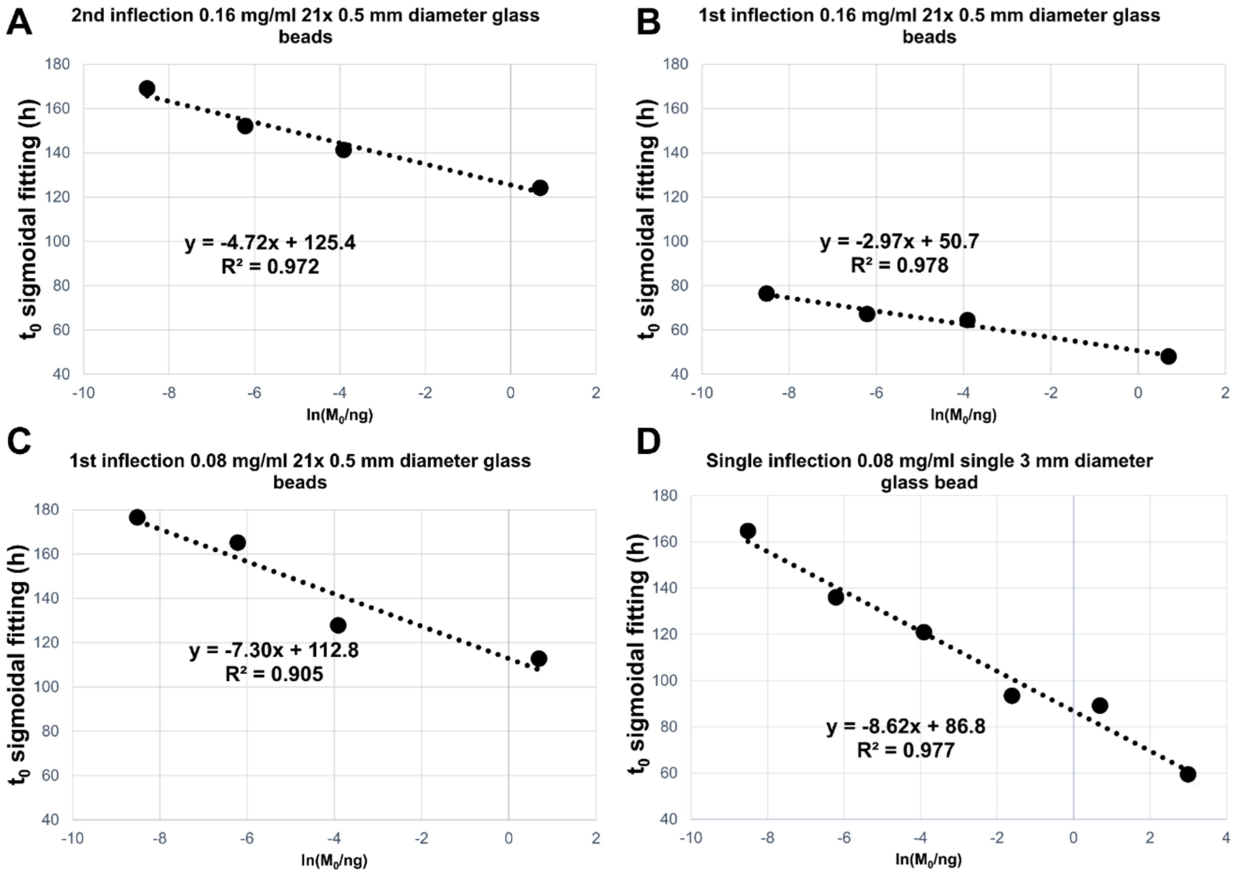

Fig. 7. Summary of linear regression analyses performed of the average (on three replicates) t_0 relative to SAAs performed in different experimental conditions. The assays were performed in 100 mM PIPES pH 6.5 (500 mM NaCl) with 40 μL of CSF (final volume of 250 μL) in the presence of different quantities of preformed aggregates. The t_0 parameters were obtained by fitting the first or the second part of the normalized fluorescence profiles with Boltzmann's sigmoidal functions. In (A) a starting concentration of 0.16 mg/mL monomeric α-syn was used together with 21 glass beads with a diameter of 0.5 mm. In (B) a starting concentration of 0.16 mg/mL monomeric α-syn was used together with 21 glass beads with a diameter of 0.5 mm. In (C) a starting concentration of 0.08 mg/mL monomeric α-syn was used together with 21 glass beads with a diameter of 0.5 mm. In (D) a starting concentration of 0.08 mg/mL monomeric α-syn was used together with 1 glass bead with a diameter of 3 mm.

of antiaggregatory compounds on α-syn fibrillization [59]. The SDS-induced α-syn fibrils are known for containing a mixture of α-helix and β-sheet and their morphology differs from that of only agitation-induced α-syn fibrils. Anyway, the two morphologies can interconvert and, thanks to temperature and strong agitation, converge into ThT responsive structures rich in β-sheet motifs [63].

5. Conclusions

The results of the experiments performed in this work showed the impact on SAAs of experimental variables like monomer concentration, addition of glass beads, size and number of glass beads, buffer pH, addition of human CSF and use of detergents. For most of the seeded experiments we usually observed the presence of two inflection points. The exact understanding of this behaviour requires further investigation. However, a possible explanation for these ThT fluorescence profiles is the transition from initially amplified oligomeric/proto-fibrillary into well-structured fibrils. Varying the starting monomer concentration affected the speed of both the seeded and unseeded aggregation. Decreasing the starting monomer concentration increased the experiment duration but produced a greater slope in seeded aggregation experiments, thus increasing the differentiation between the masses of the added seeds. By taking into account nucleated-polymerization kinetic models for protein aggregation [48, 49, 64], like the one described in Fig. 1, the monomer concentration dependence of the nucleation kinetics is of a higher order with respect of the growth of preformed aggregates. Consequently, the decrease of the monomer concentration affects more the unseeded aggregation than the seeded one.

The addition of glass beads increased both the aggregation speed and the homogeneity among replicates of seeded experiments, a result that is in accord with the results previously published by Giehm and Otzen [52]. The size and the number of the beads showed to play a major

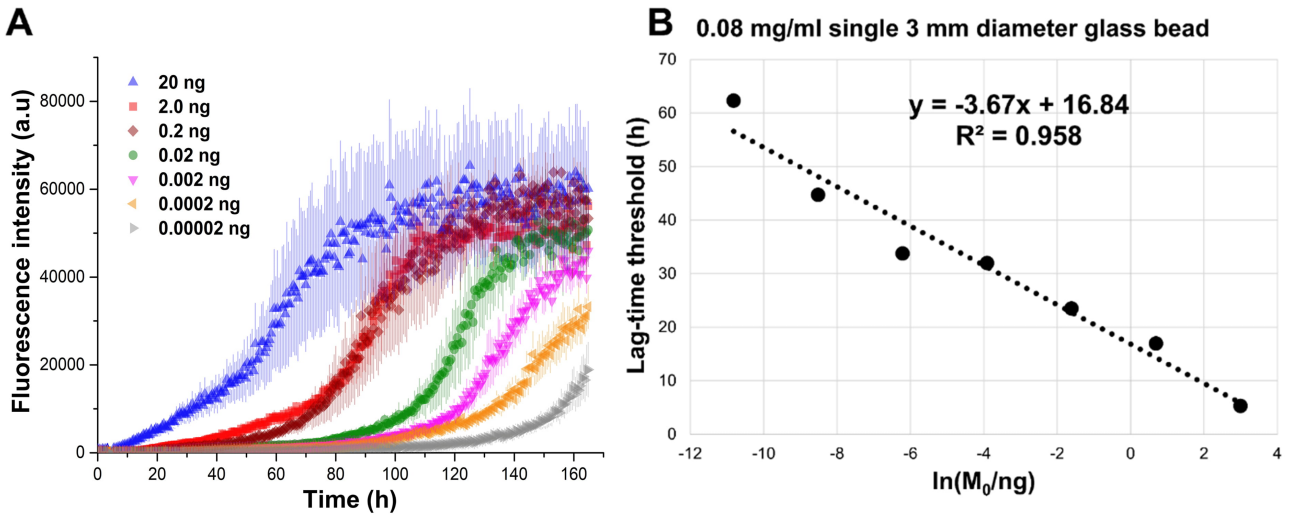

Fig. 8. SAA performed using 0.08 mg/mL of recombinant α-syn in 100 mM PIPES pH 6.5 (500 mM NaCl) with 40 μL of CSF (final volume of 250 μL) in the presence of different quantities of preformed aggregates and 1 single glass bead with a diameter of 3 mm. (A) The data shown are the averages of three replicates on a 96-wells plate while the error bars represent the standard error of the mean fluorescence value on replicates. (B) Linear regression analysis relative to the t_0 parameters obtained by fitting the whole fluorescence profiles with Boltzmann's sigmoidal functions.

Table 1. Effect of the addition of different quantities of SDS to the reaction buffer.

SDS (%)	Seeds (pg)	Lag-time (h)
0.00	0.00	>120
0.001	0.00	>120
0.005	0.00	18 ± 7
0.01	0.00	17 ± 5
0.00	0.01	>120
0.001	0.01	39.0 ± 0.7
0.005	0.01	10 ± 3
0.01	0.01	7 ± 1

The measured lag-times are shown for different experiments performed with and without seeds in the presence of SDS. In this table lag-times are represented as mean $\pm$ mean standard error calculated on three replicates.

role also in the differentiation of added seeds. By increasing the number and size of the beads, we increased the reproducibility of the assay, decreased the experiment duration and increased the differentiation among different quantities of preformed aggregates in the presence of human CSF.

These findings can be explained by considering the fragmentation kinetics [48, 64] of prion-like proteins: preformed aggregates, when fragmented, produce more template units, which can then act as new seeds for the fibrillization process. It should be also mentioned that adding too many beads or apply a too vigorous shaking or sonication may also increase water-air interfaces, which may favour the unspecific formation of amyloidogenic aggregates [55, 65]. However, in the range of the tested conditions, SAAs appear to benefit from the use of beads.

Three reaction buffers were also tested: PIPES buffer 100 mM pH 6.5 with NaCl 500 mM, PBS buffer pH 7.4 and PBS buffer pH 8.2. We observed a decrease in the aggregation speed by moving to higher pH in seeded conditions. This is in accord to the fact that, at high pH, the negatively charged monomers of α-syn experience an electrostatic repulsion that makes nucleation and the growth of aggregates energetically less favourable [42, 43]. In our experimental conditions, the addition of human CSF to our SAA reaction mix resulted in a significantly delayed aggregation of α-syn. This effect was previously observed. Indeed, in some diagnostic SAAs, efficient seeding could be obtained only after determining an optimal CSF dilution.

The addition of SDS in the reaction buffer significantly accelerated the aggregation of α-syn for the tested condition and produced a marked aggregation even in the absence of preformed seeds. This result, in accord with previous studies of Otzen and co-workers [52, 53, 63], may imply that the addition of detergents (>0.001%) may promote spontaneous nucleation of monomers, thus favouring a faster aggregation. However, comparable SDS concentrations (0.0015%) have been found to shorten the assay without compromising its specificity [28, 29, 44]. These results may then imply that SDS may not only enhance the spontaneous aggregation of α-syn but also the seeded one.

Our study has some limitations. As a limitation, we must acknowledge the usage of CSF samples coming from a single patient. This choice allowed us to minimize the effects related to biological variability of CSF samples but at the same time prevented us from characterizing possible interaction effects between the biomatrix and α-syn,

which may be relevant in diagnostic applications. Other limitations can arise from the fact that in our analysis we did not rely on fixed and already published SAA protocols. This choice was made to observe the entire aggregation kinetics in a reasonable amount of time and at the same time to highlight the effect produced by various experimental variables. However, although the effect produced by changing these variables was evaluated in specific protocols, most of the experimental variables considered influenced very general aggregation mechanisms of α-syn, thus making most of the results obtained by our analysis extendable to other protocols.

Overall, our investigation highlighted how optimization and standardization of experimental procedures for α-syn SAAs is of utmost relevance before these techniques could be routinely applied in clinical practice for diagnostic and prognostic purposes.

6. Author contributions

GB and SP conceived and designed the experiments; DR performed protein expression and purification; GB, SP and LG performed the experiments; GB analysed the data; GB wrote the first draft; FPP, LG, SP and LP critically reviewed the manuscript; MF and LP contributed reagents and materials; all authors read and revised the final version of the manuscript.

7. Ethics approval and consent to participate

All the procedures involving human subjects were performed following the Helsinki Declaration. All patients and/or their legal representatives gave informed written consent for the lumbar puncture, CSF collection, assessment, analysis, and the inclusion in the study, that was approved by the local Ethics Committee (CEAS n 1287/08), University of Perugia. CSF samples were obtained with the informed consent of all participants.

8. Acknowledgment

We thank Dr. Sara Bologna for assistance in protein expression and purification procedures.

9. Funding

GB is currently supported by the JPND bPRIDE (blood Proteins for early Discrimination of dEmentias) project. The Project leading this result has received funding under the call “JPco-fuND-2: Multinational research projects on Personalised Medicine for Neurodegenerative Diseases” (CUP number J99C18000210005).

10. Conflict of interest

The authors declare no conflict of interest.

11. References

[1] Spillantini MG, Crowther RA, Jakes R, Hasegawa M, Goedert M. α-Synuclein in filamentous inclusions of Lewy bodies from Parkinson’s disease and dementia with Lewy bodies. Proceedings of the National Academy of Sciences. 1998; 95: 6469–6473.

[2] Shahmoradian SH, Lewis AJ, Genoud C, Hench J, Moors TE, Navarro PP, *et al*. Lewy pathology in Parkinson’s disease consists of crowded organelles and lipid membranes. Nature Neuroscience. 2019; 22: 1099–1109.

[3] Bellomo G, Paciotti S, Gatticchi L, Parnetti L. The vicious cycle between α-synuclein aggregation and autophagic lysosomal dysfunction. Movement Disorders 2020; 35: 34–44.

[4] Noyce AJ, Lees AJ, Schrag A. The prediagnostic phase of Parkinson’s disease. Journal of Neurology, Neurosurgery & Psychiatry. 2016; 87: 871–878.

[5] Eusebi P, Giannandrea D, Biscetti L, Abraha I, Chiasserini D, Orso M, *et al*. Diagnostic utility of cerebrospinal fluid α-synuclein in Parkinson’s disease: a systematic review and meta-analysis. Movement Disorders. 2017; 32: 1389–1400.

[6] Majbour NK, Vaikath NN, van Dijk KD, Ardah MT, Varghese S, Vesterager LB, *et al*. Oligomeric and phosphorylated alpha-synuclein as potential CSF biomarkers for Parkinson’s disease. Molecular Neurodegeneration. 2016; 11: 7.

[7] Parnetti L, Castrioto A, Chiasserini D, Persichetti E, Tambasco N, El-Agnaf O, *et al*. Cerebrospinal fluid biomarkers in Parkinson disease. Nature Reviews Neurology. 2013; 9: 131–140.

[8] Montine TJ, Shi M, Quinn JF, Peskind ER, Craft S, Ginghina C, *et al*. CSF aβ42and tau in Parkinson’s disease with cognitive impairment. Movement Disorders. 2010; 25: 2682–2685.

[9] Parnetti L, Chiasserini D, Persichetti E, Eusebi P, Varghese S, Qureshi MM, *et al*. Cerebrospinal fluid lysosomal enzymes and alpha-synuclein in Parkinson’s disease. Movement Disorders. 2014; 29: 1019–1027.

[10] Paciotti S, Gatticchi L, Beccari T, Parnetti L. Lysosomal enzyme activities as possible CSF biomarkers of synucleinopathies. Clinica Chimica Acta. 2019; 495: 13–24.

[11] Parnetti L, Paciotti S, Farotti L, Bellomo G, Sepe FN, Eusebi P. Parkinson’s and Lewy body dementia CSF biomarkers. Clinica Chimica Acta. 2019; 495: 318–325.

[12] Gaetani L, Paolini Paoletti F, Bellomo G, Mancini A, Simoni S, Di Filippo M, *et al*. CSF and Blood Biomarkers in Neuroinflammatory and Neurodegenerative Diseases: Implications for Treatment. Trends in Pharmacological Sciences. 2020; 41: 1023–1037.

[13] Bellomo G, Paolini Paoletti F, Chipi E, Petricciuolo M, Simoni S, Tambasco N, *et al*. A/T/(N) Profile in Cerebrospinal Fluid of Parkinson’s Disease with/without Cognitive Impairment and Dementia with Lewy Bodies. Diagnostics 2020; 10: 1015.

[14] Steiner JA, Angot E, Brundin P. A deadly spread: cellular mechanisms of α-synuclein transfer. Cell Death & Differentiation. 2011; 18: 1425–1433.

[15] Tokuda T, Qureshi MM, Ardah MT, Varghese S, Shehab SAS, Kasai T, *et al*. Detection of elevated levels of α-synuclein oligomers in CSF from patients with Parkinson disease. Neurology. 2010; 75: 1766–1772.

[16] Danzer KM, Kranich LR, Ruf WP, Cagsal-Getkin O, Winslow AR, Zhu L, *et al*. Exosomal cell-to-cell transmission of alpha synuclein oligomers. Molecular Neurodegeneration. 2012; 7: 42.

[17] Ferreira NDC, Caughey B. Proteopathic Seed Amplification Assays for Neurodegenerative Disorders. Clinics in Laboratory

Medicine. 2020; 40: 257–270.
[18] Saborio GP, Permanne B, Soto C. Sensitive detection of pathological prion protein by cyclic amplification of protein misfolding. Nature. 2001; 411: 810–813.
[19] Atarashi R, Sano K, Satoh K, Nishida N. Real-time quaking-induced conversion. Prion. 2011; 5: 150–153.
[20] Dassanayake RP, Orrú CD, Hughson AG, Caughey B, Graça T, Zhuang D, *et al*. Sensitive and specific detection of classical scrapie prions in the brains of goats by real-time quaking-induced conversion. Journal of General Virology. 2016; 97: 803–812.
[21] Ferreira NC, Charco JM, Plagenz J, Orru CD, Denkers ND, Metrick MA, *et al*. Detection of chronic wasting disease in mule and white-tailed deer by RT-QuIC analysis of outer ear. Scientific Reports. 2021; 11: 7702.
[22] Kramm C, Pritzkow S, Lyon A, Nichols T, Morales R, Soto C. Detection of Prions in Blood of Cervids at the Asymptomatic Stage of Chronic Wasting Disease. Scientific Reports. 2017; 7: 17241.
[23] Green AJE. RT-QuIC: a new test for sporadic CJD. Practical Neurology. 2019; 19: 49–55.
[24] Giaccone G, Moda F. PMCA Applications for Prion Detection in Peripheral Tissues of Patients with Variant Creutzfeldt-Jakob Disease. Biomolecules 2020; 10: 405.
[25] Moda F, Gambetti P, Notari S, Concha-Marambio L, Catania M, Park K, *et al*. Prions in the Urine of Patients with Variant Creutzfeldt–Jakob Disease. New England Journal of Medicine. 2014; 371: 530–539.
[26] Fairfoul G, McGuire LI, Pal S, Ironside JW, Neumann J, Christie S, *et al*. Alpha-synuclein RT-QuIC in the CSF of patients with alpha-synucleinopathies. Annals of Clinical Translational Neurology. 2016; 3: 812–818.
[27] Shahnawaz M, Tokuda T, Waragai M, Mendez N, Ishii R, Trenkwalder C, *et al*. Development of a Biochemical Diagnosis of Parkinson Disease by Detection of α-Synuclein Misfolded Aggregates in Cerebrospinal Fluid. JAMA Neurology. 2017; 74: 163–172.
[28] Groveman BR, Orrù CD, Hughson AG, Raymond LD, Zanusso G, Ghetti B, *et al*. Rapid and ultra-sensitive quantitation of disease-associated α-synuclein seeds in brain and cerebrospinal fluid by αSyn RT-QuIC. Acta Neuropathologica Communications. 2018; 6: 7.
[29] Rossi M, Candelise N, Baiardi S, Capellari S, Giannini G, Orrù CD, *et al*. Ultrasensitive RT-QuIC assay with high sensitivity and specificity for Lewy body-associated synucleinopathies. Acta Neuropathologica. 2020; 140: 49–62.
[30] Shahnawaz M, Mukherjee A, Pritzkow S, Mendez N, Rabadia P, Liu X, *et al*. Discriminating α-synuclein strains in Parkinson's disease and multiple system atrophy. Nature. 2020; 578: 273–277.
[31] Iranzo A, Fairfoul G, Ayudhaya ACN, Serradell M, Gelpi E, Vilaseca I, *et al*. Detection of α-synuclein in CSF by RT-QuIC in patients with isolated rapid-eye-movement sleep behaviour disorder: a longitudinal observational study. Lancet Neurology. 2021; 20: 203–212.
[32] van Rumund A, Green AJE, Fairfoul G, Esselink RAJ, Bloem BR, Verbeek MM. α-Synuclein real-time quaking-induced conversion in the cerebrospinal fluid of uncertain cases of parkinsonism. Annals of Neurology. 2019; 85: 777–781.
[33] Paciotti S, Bellomo G, Gatticchi L, Parnetti L. Are We Ready for Detecting α-Synuclein Prone to Aggregation in Patients? The Case of "Protein-Misfolding Cyclic Amplification" and "Real-Time Quaking-Induced Conversion" as Diagnostic Tools. Frontiers in Neurology 2018; 9: 415.
[34] De Luca CMG, Elia AE, Portaleone SM, Cazzaniga FA, Rossi M, Bistaffa E, *et al*. Efficient RT-QuIC seeding activity for α-synuclein in olfactory mucosa samples of patients with Parkinson's disease and multiple system atrophy. Translational Neurodegeneration. 2019; 8: 24.
[35] Perra D, Bongianni M, Novi G, Janes F, Bessi V, Capaldi S, *et al*. Alpha-synuclein seeds in olfactory mucosa and cerebrospinal fluid of patients with dementia with Lewy bodies. Brain Communications. 2021; 3: fcab405.
[36] Donadio V, Wang Z, Incensi A, Rizzo G, Fileccia E, Vacchiano V, *et al*. *In Vivo* Diagnosis of Synucleinopathies. Neurology. 2021; 96: e2513–e2524.
[37] Mammana A, Baiardi S, Quadalti C, Rossi M, Donadio V, Capellari S, *et al*. RT-QuIC Detection of Pathological α-Synuclein in Skin Punches of Patients with Lewy Body Disease. Movement Disorders. 2021; 36: 2173–2177.
[38] Wang Z, Becker K, Donadio V, Siedlak S, Yuan J, Rezaee M, *et al*. Skin α-Synuclein Aggregation Seeding Activity as a Novel Biomarker for Parkinson Disease. JAMA Neurology. 2021; 78: 30.
[39] Bellomo G, Bologna S, Gonnelli L, Ravera E, Fragai M, Lelli M, *et al*. Aggregation kinetics of the aβ1–40 peptide monitored by NMR. Chemical Communications. 2018; 54: 7601–7604.
[40] Shevchik VE, Condemine G, Robert-Baudouy J. Characterization of DsbC, a periplasmic protein of Erwinia chrysanthemi and Escherichia coli with disulfide isomerase activity. EMBO Journal. 1994; 13: 2007–2012.
[41] Huang C, Ren G, Zhou H, Wang C. A new method for purification of recombinant human alpha-synuclein in Escherichia coli. Protein Expression and Purification. 2005; 42: 173–177.
[42] Bellomo G, Bologna S, Cerofolini L, Paciotti S, Gatticchi L, Ravera E, *et al*. Dissecting the Interactions between Human Serum Albumin and α-Synuclein: New Insights on the Factors Influencing α-Synuclein Aggregation in Biological Fluids. Journal of Physical Chemistry B. 2019; 123: 4380–4386.
[43] Shammas S, Knowles TJ, Baldwin A, MacPhee C, Welland M, Dobson C, *et al*. Perturbation of the Stability of Amyloid Fibrils through Alteration of Electrostatic Interactions. Biophysical Journal. 2011; 100: 2783–2791.
[44] Orrù CD, Ma TC, Hughson AG, Groveman BR, Srivastava A, Galasko D, *et al*. A rapid α-synuclein seed assay of Parkinson's disease CSF panel shows high diagnostic accuracy. Annals of Clinical and Translational Neurology. 2021; 8: 374–384.
[45] Teunissen CE, Petzold A, Bennett JL, Berven FS, Brundin L, Comabella M, *et al*. A consensus protocol for the standardization of cerebrospinal fluid collection and biobanking. Neurology. 2009; 73: 1914–1922.
[46] Chiasserini D, Biscetti L, Farotti L, Eusebi P, Salvadori N, Lisetti V, *et al*. Performance Evaluation of an Automated ELISA System for Alzheimer's Disease Detection in Clinical Routine. Journal of Alzheimer's Disease. 2016; 54: 55–67.
[47] Arosio P, Cukalevski R, Frohm B, Knowles TPJ, Linse S. Quantification of the Concentration of aβ42 Propagons during the Lag Phase by an Amyloid Chain Reaction Assay. Journal of the American Chemical Society. 2014; 136: 219–225.
[48] Pöschel T, Brilliantov NV, Frömmel C. Kinetics of Prion Growth. Biophysical Journal. 2003; 85: 3460–3474.
[49] Ferrone F. Analysis of protein aggregation kinetics. Methods in Enzymology. 1999; 309: 256–274.
[50] Törnquist M, Michaels TCT, Sanagavarapu K, Yang X, Meisl G, Cohen SIA, *et al*. Secondary nucleation in amyloid formation. Chemical Communications. 2018; 54: 8667–8684.
[51] Buell AK, Galvagnion C, Gaspar R, Sparr E, Vendruscolo M, Knowles TPJ, *et al*. Solution conditions determine the relative importance of nucleation and growth processes in α-synuclein aggregation. Proceedings of the National Academy of Sciences. 2014; 111: 7671–7676.
[52] Giehm L, Otzen DE. Strategies to increase the reproducibility of protein fibrillization in plate reader assays. Analytical Biochemistry. 2010; 400: 270–281.
[53] Giehm L, Lorenzen N, Otzen DE. Assays for α-synuclein aggregation. Methods. 2011; 53: 295–305.
[54] Hoyer W, Antony T, Cherny D, Heim G, Jovin TM, Subramaniam V. Dependence of alpha-synuclein aggregate morphol-

ogy on solution conditions. Journal of Molecular Biology. 2002; 322: 383–393.
[55] Candelise N, Schmitz M, Thüne K, Cramm M, Rabano A, Zafar S, *et al*. Effect of the micro-environment on α-synuclein conversion and implication in seeded conversion assays. Translational Neurodegeneration. 2020; 9: 5.
[56] Watanabe-Nakayama T, Nawa M, Konno H, Kodera N, Ando T, Teplow DB, *et al*. Self- and Cross-Seeding on α-Synuclein Fibril Growth Kinetics and Structure Observed by High-Speed Atomic Force Microscopy. ACS Nano. 2020; 14: 9979–9989.
[57] Concha-Marambio L, Shahnawaz M, Soto C. Detection of Misfolded α-Synuclein Aggregates in Cerebrospinal Fluid by the Protein Misfolding Cyclic Amplification Platform. Methods in Molecular Biology. 2019; 1948: 35–44.
[58] Bargar C, Wang W, Gunzler SA, LeFevre A, Wang Z, Lerner AJ, *et al*. Streamlined alpha-synuclein RT-QuIC assay for various biospecimens in Parkinson's disease and dementia with Lewy bodies. Acta Neuropathologica Communications. 2021; 9: 62.
[59] Paslawski W, Zareba-Paslawska J, Zhang X, Hölzl K, Wadensten H, Shariatgorji M, *et al*. α-synuclein−lipoprotein interactions and elevated ApoE level in cerebrospinal fluid from Parkinson's disease patients. Proceedings of the National Academy of Sciences. 2019; 116: 15226–15235.
[60] Brown JWP, Meisl G, Knowles TPJ, Buell AK, Dobson CM, Galvagnion C. Kinetic barriers to α-synuclein protofilament formation and conversion into mature fibrils. Chemical Communications. 2018; 54: 7854–7857.
[61] Bhak G, Lee S, Kim T, Lee J, Yang JE, Joo K, *et al*. Morphological Evaluation of Meta-stable Oligomers of α-Synuclein with Small-Angle Neutron Scattering. Scientific Reports. 2018; 8: 14295.
[62] Adler J, Scheidt HA, Lemmnitzer K, Krueger M, Huster D. N-terminal lipid conjugation of amyloid β (1–40) leads to the formation of highly ordered N-terminally extended fibrils. Physical Chemistry Chemical Physics. 2017; 19: 1839–1846.
[63] Giehm L, Oliveira CLP, Christiansen G, Pedersen JS, Otzen DE. SDS-induced fibrillation of alpha-synuclein: an alternative fibrillation pathway. Journal of Molecular Biology. 2010; 401: 115–133.
[64] Cohen SIA, Vendruscolo M, Welland ME, Dobson CM, Terentjev EM, Knowles TPJ. Nucleated polymerization with secondary pathways. i. Time evolution of the principal moments. The Journal of Chemical Physics. 2011; 135: 065105.
[65] Schladitz C, Vieira EP, Hermel H, Möhwald H. Amyloid-beta-sheet formation at the air-water interface. Biophysical Journal. 1999; 77: 3305–3310.

Supplementary material: Supplementary material associated with this article can be found, in the online version, at https://www.fbscience.com/Landmark/articles/10.52586/5010.

Keywords: α-synuclein; PMCA; RT-QuIC; SAAs; Influencing factors

Send correspondence to:

Giovanni Bellomo, Laboratory of Clinical Neurochemistry, Section of Neurology, Department of Medicine and Surgery, University of Perugia, 06132 Perugia, Italy, E-mail: giovanni.bellomo@unipg.it

Lucilla Parnetti, Laboratory of Clinical Neurochemistry, Section of Neurology, Department of Medicine and Surgery, University of Perugia, 06132 Perugia, Italy, E-mail: lucilla.parnetti@unipg.it